Xiao-Fan Zhang and Qing-Guo Meng*

Crystal structure of (*E*)-2-((2-methoxy-3-pyridyl) methylene)-7-fluoro-3,4-dihydronaphthalen-1(2*H*)-one, $C_{17}H_{14}FNO_2$

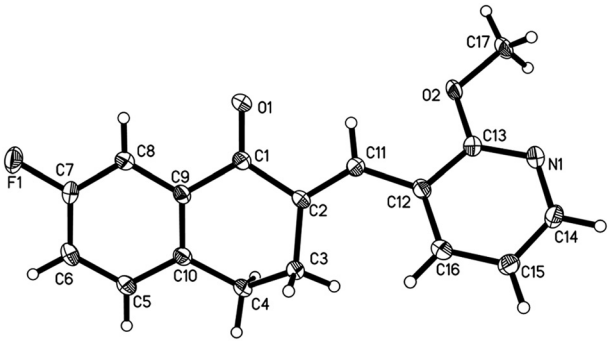

https://doi.org/10.1515/ncrs-2020-0603
Received November 18, 2020; accepted December 30, 2020; published online January 28, 2021

Abstract

$C_{17}H_{14}FNO_2$, monoclinic, $P2_1/c$ (no. 14), a = 14.0279(13) Å, b = 7.0527(5) Å, c = 14.4150(16) Å, β = 113.165(12)°, V = 1311.2(2) Å^3, Z = 4, $R_{gt}(F)$ = 0.0524, $wR_{ref}(F^2)$ = 0.1358, T = 100 K.

CCDC no.: 2039247

The molecular structure is shown in the Figure. Table 1 contains crystallographic data and Table 2 contains the list of the atoms including atomic coordinates and displacement parameters.

***Corresponding author: Qing-Guo Meng**, School of Pharmacy, Collaborative Innovation Center of Advanced Drug Delivery System and Biotech Drugs in Universities of Shandong, Key Laboratory of Molecular Pharmacology and Drug Evaluation (Yantai University), Ministry of Education, Yantai University, Yantai, P. R. China, E-mail: qinggmeng@163.com

Xiao-Fan Zhang, School of Pharmacy, Collaborative Innovation Center of Advanced Drug Delivery System and Biotech Drugs in Universities of Shandong, Key Laboratory of Molecular Pharmacology and Drug Evaluation (Yantai University), Ministry of Education, Yantai University, Yantai, P. R. China. https://orcid.org/0000-0003-0674-2008

Table 1: Data collection and handling.

Crystal:	Colourless block
Size:	0.15 × 0.13 × 0.11 mm
Wavelength:	Mo *K*α radiation (0.71073 Å)
μ:	0.10 mm^{-1}
Diffractometer, scan mode:	SuperNova
θ_{max}, completeness:	25.5°, 99%
$N(hkl)_{measured}$, $N(hkl)_{unique}$, R_{int}:	4957, 2438, 0.031
Criterion for I_{obs}, $N(hkl)_{gt}$:	$I_{obs} > 2\ \sigma(I_{obs})$, 1910
$N(param)_{refined}$:	191
Programs:	CrysAlis^{PRO} [1], SHELX [2,3]

Source of material

7-Fluoro-3,4-dihydro-1(2*H*)-naphthalenone (0.7 g, 4.26 mmol) and 2-fluoro-3-formylpyridine (0.53 g, 4.26 mmol) were dissolved in 10 mL methanol. A sodium hydroxide aqueous solution (25%) was added to the mixture and stirred for 3 h at room temperature. The response endpoint was detected by thin layer chromatography (TLC, 254 nm). When 7-fluoro-3,4-dihydro-1(2*H*)-naphthalenone disappeared, the precipitate was filtered from the reaction mixture and dissolved with dichloromethane. The organic phase was washed respectively with deionized water and brine, dried over anhydrous sodium sulfate and condensed under vacuum. The crude product was purified by silica-gel column chromatography (petroleum ether: ethyl acetate = 10:1, *v*/*v*). Single crystal was obtained under ambient conditions via solvent evaporation in the mixed solvents of dichloromethane and methanol (1:1, *v*/*v*) and drying under vacuo at 333 K for 3 h.

Experimental details

The H atoms were placed in idealized positions and treated as riding on their parent atoms, with d(C—H) = 0.96 Å (methyl), U_{iso}(H) = 1.5U_{eq}(C), and d(C—H) = 0.97 Å (methylene), U_{iso}(H) = 1.2U_{eq}(C), and d(C—H) = 0.93 Å (aromatic), U_{iso}(H) = 1.2U_{eq}(C).

Table 2: Fractional atomic coordinates and isotropic or equivalent isotropic displacement parameters (Å^2).

	x	*y*	*z*	U_{iso}*/U_{eq}
C1	0.47372 (16)	0.5363 (3)	0.60726 (15)	0.0216 (5)
C2	0.52721 (16)	0.7232 (3)	0.64029 (15)	0.0206 (5)
C3	0.46085 (16)	0.8992 (3)	0.62279 (16)	0.0229 (5)
H3A	0.447439	0.948526	0.555991	0.027*
H3B	0.498772	0.995243	0.671525	0.027*
C4	0.35743 (16)	0.8621 (3)	0.63186 (17)	0.0244 (5)
H4A	0.369926	0.842488	0.702299	0.029*
H4B	0.313485	0.972875	0.608510	0.029*
C5	0.19429 (16)	0.6850 (3)	0.52630 (16)	0.0252 (5)
H5	0.155941	0.791073	0.528701	0.030*
C6	0.14291 (17)	0.5233 (3)	0.47724 (17)	0.0277 (5)
H6	0.070919	0.520037	0.446411	0.033*
C7	0.20129 (17)	0.3674 (3)	0.47532 (16)	0.0250 (5)
C8	0.30745 (16)	0.3677 (3)	0.51677 (16)	0.0228 (5)
H8	0.344735	0.260862	0.513213	0.027*
C9	0.35843 (16)	0.5333 (3)	0.56472 (15)	0.0201 (5)
C10	0.30175 (16)	0.6922 (3)	0.57194 (15)	0.0213 (5)
C11	0.63138 (16)	0.7192 (3)	0.68050 (15)	0.0220 (5)
H11	0.659874	0.598055	0.691636	0.026*
C12	0.70752 (16)	0.8725 (3)	0.70972 (16)	0.0216 (5)
C13	0.81155 (16)	0.8328 (3)	0.77370 (16)	0.0225 (5)
C14	0.86833 (17)	1.1292 (3)	0.75901 (17)	0.0270 (5)
H14	0.922433	1.215867	0.774860	0.032*
C15	0.77038 (17)	1.1868 (3)	0.69688 (16)	0.0254 (5)
H15	0.758412	1.310006	0.672016	0.031*
C16	0.69004 (17)	1.0579 (3)	0.67206 (16)	0.0243 (5)
H16	0.623403	1.094834	0.629762	0.029*
C17	0.93629 (16)	0.6116 (4)	0.87542 (18)	0.0304 (6)
H17A	0.980048	0.637150	0.839771	0.046*
H17B	0.942323	0.480371	0.894641	0.046*
H17C	0.957201	0.689483	0.934725	0.046*
F1	0.15087 (10)	0.2050 (2)	0.42968 (10)	0.0362 (4)
N1	0.88976 (14)	0.9528 (3)	0.79815 (13)	0.0254 (5)
O1	0.52231 (11)	0.3891 (2)	0.61177 (12)	0.0296 (4)
O2	0.83063 (11)	0.6529 (2)	0.81134 (11)	0.0279 (4)

Comment

Microglia become activated under brain injury and immunological stimuli and undergo several alterations from a resting state to an active state. This activation and consequent neuroinflammation are substantially involved in the pathological development of inflammatory neurodegenerative diseases in the central nervous system (CNS) [4, 5]. It has been reported that pro-inflammatory cytokines [tumor necrosis factor (TNF-α), interleukin (IL)-6, IL-1β] secreted from M1 microglia increase blood-brain barrier (BBB) permeability by activating the nuclear factor kappa B (NF-κB) signaling pathway during inflammatory neurodegenerative diseases in CNS [6–8]. Concomitantly, the disruption of the blood-brain barrier can result in severe inflammatory response that aggravates the brain injury [9]. In addition, activated microglia can produce reactive oxygen species (ROS), which may indirectly induce neuroinflammation by activating NF-κB [10, 11]. Therefore, NF-κB inhibitor with anti-neuroinflammatory activity may represent a therapeutic option for the treatment of inflammatory neurodegenerative diseases [12–14].

3,4-Dihydronaphthalen-1(2*H*)-one (DHN) derivatives with antitumor and anti-inflammatory activities have been investigated as novel modulators of allergic and inflammatory responses [15, 16]. Our interests lie in developing these derivatives as anti-neuroinflammatory drugs. In this study, we designed and synthesized a new DHN derivative through Claisen–Schmidt condensation reaction.

Single crystals of the title compound were prepared under ambient conditions, with crystallization obtained via solvent evaporation in the mixed solvents of methanol and dichloromethane. Single-crystal structure analysis revealed that the title compound, here termed **XF-1-4-2**, crystallized in the monoclinic space group $P2_1/c$. The ORTEP diagram is presented in the Figure. There is only a drug molecule in the asymmetric unit. With respect to the C(12) = C(11) olefinic bonds, 2-methoxyphenyl and carbonyl groups adopt the *E* stereochemistry [17]. Because of the distorting effect of 3,4-dihydrobenzo[b]oxepin-5(2*H*)-one, the 7-fluorophenyl and 2-methoxyphenyl groups are not coplanar with each other, with a dihedral angle of approximately 37.8(3)°. This twisted configuration may increase the likelihood of interactions with bioactive molecules or the purposes of creating more potent biological activity [18, 19]. All geometric parameters are in the expected ranges [20]. Displacement ellipsoids are drawn at the 50% probability level.

Author contributions: All the authors have accepted responsibility for the entire content of this submitted manuscript and approved submission.

Research funding: Science and Technology Innovation Development Plan of Yantai (No. 2020XDRH105) and the National Natural Science Foundation of China (No. 81473104).

Conflict of interest statement: The authors declare no conflicts of interest regarding this article.

References

1. Rigaku OD. *CrysAlisPRO*; Rigaku Oxford Diffraction Ltd: Yarnton, Oxfordshire, England, 2017.
2. Sheldrick G. M. A short history of *SHELX*. *Acta Crystallogr.* 2008, *A64*, 112–122.
3. Sheldrick G. M. Crystal structure refinement with *SHELXL*. *Acta Crystallogr.* 2015, *C71*, 3–8.
4. Goldmann T., Prinz M. Role of microglia in CNS autoimmunity. *Clin. Dev. Immunol.* 2013, *2013*, 208093.
5. Li N., Xin W. Y., Yao B. R., Wang C. H., Cong W., Zhao F., Li H. J., Hou Y., Meng Q. G., Hou G. G. Novel dissymmetric 3,5-bis(arylidene)-4-piperidones as potential antitumor agents with biological evaluation *in vitro* and *in vivo*. *Eur. J. Med. Chem.* 2018, *147*, 21–33.
6. Correale J. The role of microglial activation in disease progression. *Mult. Scler. J.* 2014, *20*, 1288–1295.
7. Zhang J. Q., Zhang Q., Xu Y. R., Li H. X., Zhao F. L., Wang C. M., Liu Z., Liu P., Liu Y. N., Meng Q. G., Zhao F. Synthesis and *in vivo* anti-inflammatory activity of C20 epimeric ocotillol-type triterpenes and protopanaxadiol. *Planta Med.* 2019, *85*, 292–301.
8. Wang C. M., Liu J., Deng J. Q., Wang J. Z., Weng W. Z., Chu H. X., Meng Q. G. Advances in the chemistry, pharmacological diversity, and metabolism of 20(*R*)-ginseng saponins. *J. Ginseng Res.* 2020, *44*, 14–23.
9. Gao C. L., Hou G. G., Liu J., Ru T., Xu Y. Z., Zhao S. Y., Ye H., Zhang L. Y., Chen K. X., Guo Y. W., Pang T., Li X. W. Synthesis and target identification of benzoxepane derivatives as potential anti-neuroinflammatory agents for ischemic stroke. *Angew. Chem. Int. Ed.* 2020, *59*, 2429–2439.
10. Bi Y., Yang J., Ma C., Liu Z. Y., Zhang T. T., Zhang X. C., Lu J., Meng Q. G. Design, synthesis and *in vitro* NO-releasing activities of ocotillol-type furoxans. *Pharmazie* 2015, *70*, 213–218.
11. Liu J., Xu Y. R., Yang J. J., Wang W. Z., Zhang J. Q., Zhang R. M., Meng Q. G. Discovery, semisynthesis, biological activities, and metabolism of ocotillol-type saponins. *J. Ginseng Res.* 2017, *41*, 373–378.
12. Sun Y., Zhou Y. Q., Liu Y. K., Zhang H. Q., Hou G. G., Meng Q. G., Hou Y. Potential anti-neuroinflammatory NF-κB inhibitors based on 3,4-dihydronaphthalen-1(2*H*)-one derivatives. *J. Enzyme Inhib. Med. Chem.* 2020, *35*, 1631–1640.
13. Zeng K. W., Wang S., Dong X., Jiang Y., Tu P. F. Sesquiterpene dimer (DSF-52) from Artemisia argyi inhibits microglia-mediated neuroinflammation *via* suppression of NF-κB, JNK/p38 MAPKs and Jak2/Stat3 signaling pathways. *Phytomedicine* 2014, *21*, 298–306.
14. Sun Y., Gao Z. F., Yan W. B., Yao B. R., Xin W. Y., Wang C. H., Meng Q. G., Hou G. G. Discovery of novel NF-κB inhibitor based on scaffold hopping: 1,4,5,6,7,8-hexahydropyrido[4,3-*d*] pyrimidine. *Eur. J. Med. Chem.* 2020, *198*, 112366.
15. Barlow J. W., Zhang T., Woods O., Byrne A. J., Walsh J. J. Novel mast cell-stabilising amine derivatives of 3,4 dihydronaphthalen-1(2*H*)-one and 6,7,8,9-tetrahydro-5*H*-benzo[7]annulen-5-one. *Med. Chem.* 2011, *7*, 213–223.
16. Kirby A. J., Le Lain R., Maharlouie F., Mason P., Nicholls P. J., Smith H. J., Simons C. Inhibition of retinoic acid metabolising enzymes by 2-(4-aminophenylmethyl)-6-hydroxy-3,4-dihydronaphthalen-1(2*H*)-one and related compounds. *J. Enzyme Inhib. Med. Chem.* 2003, *18*, 27–33.
17. Li N., Xin W. Y., Yao B. R., Wang C. H., Cong W., Zhao F., Li H. J., Hou Y., Meng Q. G., Hou G. G. Novel dissymmetric 3,5-bis(arylidene)-4-piperidones as potential antitumor agents with biological evaluation *in vitro* and *in vivo*. *Eur. J. Med. Chem.* 2018, *147*, 21–33.
18. Yang Q. W., Wang N., Zhang J., Chen G., Xu H., Meng Q. G., Du Y., Yang X., Fan H. Y. *In vitro* and *in silico* evaluation of stereoselective effect of ginsenosideisomers on platelet P2Y12 receptor. *Phytomedicine* 2019, *64*, 152899.
19. Li N., Yao B. Y., Wang C. H., Meng Q. G., Hou G. G. Synthesis, crystal structure and activity evaluation of novel 3,4-dihydro-1-benzoxepin-5(2*H*)-one derivatives as protein– tyrosine kinase (PTK) inhibitors. *Acta Crystallogr.* 2017, *C73*, 1003–1009.
20. Sun Y., Gao Z., Wang C., Hou G. Synthesis, crystal structures and anti-inflammatory activity of fluorine-substituted 1,4,5,6-tetrahydrobenzo[*h*]quinazolin-2-amine derivatives. *Acta Crystallogr.* 2019, *C75*, 1157–1165.